Nanoscale Advances

PAPER

View Article Online
View Journal | View Issue

Check for updates

Cite this: *Nanoscale Adv.*, 2022, **4**, 4782

Non-contact friction energy dissipation *via* hysteretic behavior on a graphite surface

Chong Wang,[a] Huixian Liu,[a] Jiangcai Wang,[a] Yishu Han,[a] Zejun Sun,[a] Haowen Xu,[b] Huan Liu,*[a] Dameng Liu *[a] and Jianbin Luo*[a]

For non-contact friction, energy is usually dissipated through phonon excitation, Joule dissipation and van der Waals friction. Although some new dissipation mechanisms related to the quantum phenomenon have been discovered, the contribution of hysteretic behavior to non-contact friction energy dissipation is lacking in research. In this paper, the distance dependence of non-contact friction on the graphite surface is studied by using a quartz tuning fork with lateral vibration in the atmosphere. It is found that energy dissipation begins to increase when the distance is less than 2 nm, showing the form of phonon dissipation. However, when the distance is further decreased, the dissipation deviates from phonon dissipation and presents a huge friction energy dissipation peak, which is caused by the hysteretic behavior between the vibration of the surface atoms and the oscillation of the tip. This work expands the understanding of the energy dissipation mechanism of non-contact friction.

Received 16th July 2022
Accepted 25th September 2022

DOI: 10.1039/d2na00459c

rsc.li/nanoscale-advances

Open Access Article. Published on 29 September 2022. Downloaded on 6/21/2026 10:24:36 AM.
This article is licensed under a Creative Commons Attribution-NonCommercial 3.0 Unported Licence.

Introduction

About 30% of the world's primary energy is consumed by friction, and 80% of mechanical parts fail due to wear and tear.[1,2] It is a key problem to explore the mechanism of energy dissipation in friction and control the energy dissipation channel from the source. Normally, friction occurs between two surfaces that are in contact. Interestingly, when two objects separated by a few nanometers move relative to each other, there is still little resistance, which is called non-contact friction.[3,4] Non-contact friction is a common phenomenon which has been observed in conductors, semiconductors and insulators, and the associated energy dissipation is closely related to phonons, electrons, defects and structural phase transitions.[5–18] The study of non-contact friction is of great significance to explore the origin of friction and break the detection limit of precision instruments.[19] At present, the tuning fork non-contact lateral force microscope can detect lateral non-contact friction sensitively at a very small tip-sample distance with the help of a high-quality factor quartz tuning fork, and it has become a powerful tool to study the energy dissipation mechanism of non-contact friction.[20–26]

There are three typical dissipation forms of non-contact friction, which are phonon excitation, Joule dissipation and van der Waals friction.[27] Recently, a number of new dissipation mechanisms have been discovered, which induce striking non-contact friction energy dissipation peaks. For instance, due to the disturbance of the tip, phase slip of the charge-density-wave (CDW) occurs on the surface of $NbSe_2$ at a low temperature, which produces hysteretic behavior of the CDW phase and introduces huge dissipation peaks at a certain tip-sample distance and bias.[28] Similarly, at a low temperature, the oscillation of the tip can induce charge and spin state transitions of oxygen vacancy defects on the $SrTiO_3$ surface, leading to significant mechanical dissipation peaks.[29] In addition, a new mechanism due to single electron resonance tunneling to image potential states has also been observed on the Bi_2Te_3 topological insulator surface.[30] However, friction exists not only in extreme environments such as an ultra-high vacuum and ultra-low temperature, but also in atmospheric environments more widely. Although some quantum phenomena related to non-contact dissipation vanish in the atmospheric, phonon excitation and lattice deformation which may have hysteretic behavior with the oscillation of the tip still exist on the sample surface, whose significance is poorly explored.

In this paper, we detect a large non-contact friction energy dissipation peak on the surface of graphite by using a homebuilt tuning fork non-contact lateral force microscope in the atmosphere. We speculate that the dissipation peak is due to the hysteretic behavior between the vibration of the surface atoms and the oscillation of the tip. This work helps to better understand the non-contact friction energy dissipation mechanism.

Results and discussion

Experimental setup and sample characterization

Fig. 1(a) shows the schematic diagram of the homebuilt tuning fork non-contact lateral force microscope. The microscope uses

[a]State Key Laboratory of Tribology, Tsinghua University, Beijing 100084, China. E-mail: liuhuansklt@163.com; ldm@tsinghua.edu.cn; luojb@mail.tsinghua.edu.cn
[b]Institue for Advanced Materials and Technology, University of Science and Technology Beijing, Beijing 100083, China

© 2022 The Author(s). Published by the Royal Society of Chemistry

Open Access Article. Published on 29 September 2022. Downloaded on 6/21/2026 10:24:36 AM.
This article is licensed under a Creative Commons Attribution-NonCommercial 3.0 Unported Licence.

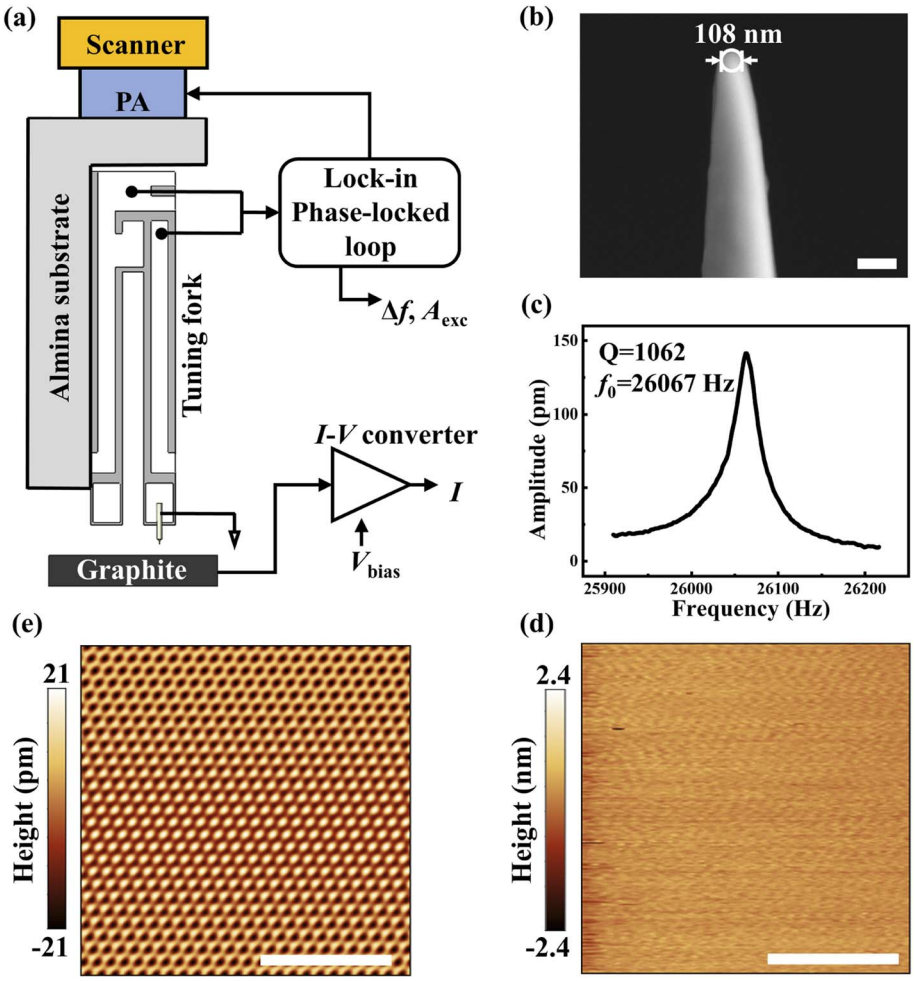

Fig. 1 (a) Schematic diagram of experimental installation. The quartz tuning fork is fixed on an alumina substrate and oscillates at a constant amplitude parallelly to the graphite surface under the excitation of PA. The scanning tube drives the quartz tuning fork and tip towards the sample surface, during which the frequency offset Δf, excitation amplitude A_{exc}, and tunneling current I are recorded as a function of the tip-sample distance d; (b) scanning electron image of the electrochemically etched tungsten tip used in the experiment. The scale bar is 200 nm; (c) Amplitude resonance curve. The intrinsic frequency $f_0 = 26\,067$ Hz and quality factor of sensor $Q = 1062$; (d) STM topography of graphite obtained in constant current mode. Surface roughness $R_a = 0.13$ nm and the scale bar is 2 nm; (e) atomic image obtained from (d) after FFT. The scale bar is 2 nm.

a piezoelectric scanning tube to drive the tip while the sample remains stationary. Below the scanning tube is a piezo actuator (PA) that vibrates horizontally to excite the quartz tuning fork to oscillate. The quartz tuning fork acts as a force sensor. One of its cantilevers is fixed to an alumina substrate by high-strength epoxy adhesive, while an electrochemically etched tungsten tip is glued to the front end of the other free cantilever to increase the quality factor. To extract the tunneling current while detecting the lateral interaction, a soft gold wire with a diameter of 12.5 μm and a length of approximately 1 mm is used to ground the tip, and bias is applied on the sample surface. This method can detect the tunneling current between the tip and sample without affecting the vibration of the quartz tuning fork to the greatest extent. Before the experiment, the sensor has been calibrated by analyzing the thermal noise spectrum[31] (see Methods). The OC4 module of a commercial Nanonis controller is applied to control PA which excites the quartz tuning fork to vibrate at a certain frequency and amplitude through a lock-in phase-locked loop (PLL) feedback system, and maintain a constant amplitude $A = 300$ pm. The cantilever of the quartz tuning fork is placed perpendicular to the sample, so the tip oscillates parallelly to the sample surface, allowing direct detection of the lateral interaction between the tip and the sample.

The tip used in the experiment was obtained by electrochemically etching 75 μm tungsten wire in 2 mol L^{-1} KOH solution. As shown in Fig. 1(b), a field emission scanning electron microscope (HITACHI SU8220) was used to image the tip, and the tip radius was about 54 nm. The elastic constant of the quartz tuning fork is approximately 10^4 N m^{-1}. After installing the tungsten tip and gold wire, we measured the response of the sensor's amplitude to excitation frequency in the atmosphere with the help of an OC4 module. By Gaussian function fitting, we obtained the intrinsic frequency $f_0 = 26\,067$ Hz and the quality factor of sensor $Q = 1062$, as shown in Fig. 1(c).

© 2022 The Author(s). Published by the Royal Society of Chemistry

Open Access Article. Published on 29 September 2022. Downloaded on 6/21/2026 10:24:36 AM.
This article is licensed under a Creative Commons Attribution-NonCommercial 3.0 Unported Licence.

The sample was fresh, atomically flat, commercial highly oriented cleaved graphite crystals (HOPG) that had been mechanically cleaved. Using tunneling current as the feedback signal, the surface morphology of the sample was measured in constant current mode. As shown in Fig. 1(d), the surface of the sample is atomically flat with a surface roughness of R_a = 0.13 nm, and no obvious contaminant or other structural defects are found. Fig. 1(e) shows the atomic lattice diagram of Fig. 1 (d) filtered by FFT. On this basis, we carried out non-contact friction measurements.

Tip oscillation induced phonon dissipation on a graphite surface

Under the open-loop control, the variation of the non-contact friction coefficient Γ_{int} and the friction-induced elastic constant k_{int} with the tip-sample distance d were investigated. As shown in Fig. 2(a), the probe always oscillates at the intrinsic frequency and constant amplitude, and we control the tip to approach the sample surface gradually from a large separation until it stops when the tunneling current reaches a preset value. At a large distance (>100 nm), the oscillation of the tip is not

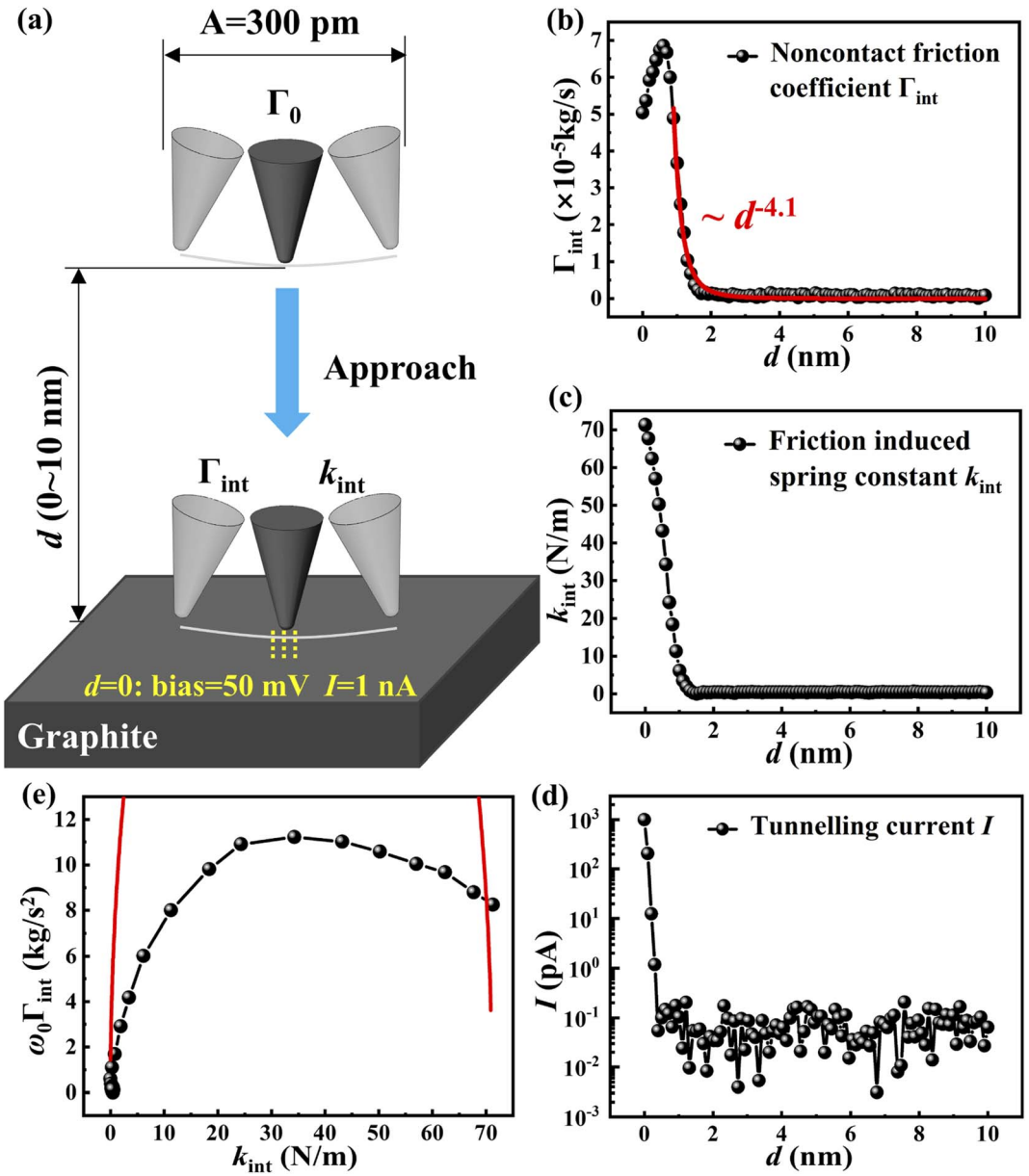

Fig. 2 (a) Schematic diagram of the experimental process. Under the open-loop control, the tip oscillates with intrinsic frequency and constant amplitude and gradually approaches the sample surface from a long distance until the tunneling current reaches the set value; (b) distance dependence of non-contact friction coefficient Γ_{int} between the tip and graphite surface; (c) distance dependence of the friction-induced elastic constant k_{int}. Data were obtained at room temperature and atmosphere; (d) tunneling current *versus* distance spectrum taken simultaneously with (b) and (c); (e) the black curve is $\omega_0\Gamma_{int}$ as a function of k_{int} with data from (b) and (c). The red lines are the lower part of the semicircle fitting of the experimental data and the center of the circle is on the x-axis.

© 2022 The Author(s). Published by the Royal Society of Chemistry

Open Access Article. Published on 29 September 2022. Downloaded on 6/21/2026 10:24:36 AM.
This article is licensed under a Creative Commons Attribution-NonCommercial 3.0 Unported Licence.

affected by the sample and the damping comes only from the internal friction Γ_0 of the cantilever. In the process of approaching, energy dissipation occurs due to the interaction. In order to maintain the constant amplitude of the quartz tuning fork, PLL must increase the excitation amplitude A_{exc}. Therefore, A_{exc} directly reflects the non-conservative interaction, while the frequency offset Δf reflects the conservative interaction.[22,32] Here, the non-conservative interaction refers to the interaction which causes energy dissipation in the tip-sample junction, while the conservative interaction on the contrary, refers to those that do not cause energy dissipation. Γ_{int} and k_{int} can be calculated using A_{exc} and Δf:[5,33]

$$\Gamma_{int} = \Gamma_0\left(\frac{A_{exc}(d)}{A_{exc,0}} - \frac{f(d)}{f_0}\right) \quad (1)$$

$$k_{int} = \frac{2k_0\Delta f}{f_0} \quad (2)$$

where $A_{exc}(d)$ is the excitation amplitude related to the tip-sample distance, and $A_{exc,0}$ is the excitation amplitude when the tip and sample have no interaction at large separation; $f(d) = f_0 + \Delta f$ is the vibration frequency of the cantilever related to distance; $\Gamma_0 = k_0/2\pi f_0 Q$ is the internal friction coefficient of the cantilever. In our experiment, $d = 0$ was defined as the distance where the bias was 50 mV and the tunneling current was 1 nA. At this point, the tunneling resistance is 50 MΩ, which is much larger than the quantum resistance $h/2e^2$when point contact is formed.[34] At this time, electrical conduction was mainly dominated by the tunneling current, and there was no physical contact between the tip and the sample.

Fig. 2(b) and (c) show that Γ_{int} and k_{int} on the graphite surface gradually increase with the decrease of the tip-sample distance at $d < 2$ nm. The order of magnitude of Γ_{int} is 10^{-5} kg s^{-1}. Unlike k_{int} which increases monotonically as d decreases, Γ_{int} shows a huge peak at $d \sim 0.6$ nm. At the same time, when it reaches its peak, no tunneling current is detected [Fig. 2(d)], indicating that the tip does not form a physical contact with the sample at this time, that is, the maximum of the friction coefficient is not from the collision with the sample surface. Similar results were also observed by Saitoh *et al.*[20] The difference was that they observed the dissipation peak at a low temperature, while we observed the dissipation peak at room temperature. In addition, the non-contact friction observed by us increased significantly at $d < 2$ nm, while the friction observed by them began to increase at $d < 15$ nm. We have observed a more localized non-contact interaction in space.

Volokitin *et al.* found that for a spherical tip oscillating parallel to the elastic surface, the non-contact friction coefficient is proportional to $F^2(d)$ which is the static force resulting from the interaction between the tip and the sample surface.[35] According to Lifshitz theory, the elastic stress $F(d)$ caused by van der Waals interaction gives rise to the static force to be proportional to d^{-2}, and therefore the phonon friction coefficient to be proportional to d^{-4}.[36] By fitting the data in Fig. 2(b) with power exponents, we find that the non-contact friction coefficient is proportional to $d^{-4.1\pm0.1}$ within the range 1 nm < d < 10 nm, which is in good agreement with the above prediction, indicating that phonon friction is the main dissipation mechanism at this time. However, when the tip gets closer to the sample, the dissipation increases further and then decreases gradually, deviating from the phonon dissipation. Therefore, a new dissipation mechanism appears at closer separation.

Possible reasons for the maximum of Γ_{int} as the tip-sample distance decreases are discussed below. First of all, surface contaminants and structure defects can induce dissipation.[37] However, the STM topography shows that the sample surface is atomically smooth and clean, and no obvious contaminants and structure defects are found. In addition, the effect of a water film and adsorbed contamination on dissipation has been discussed in previous studies where the dissipation started to increase at $d > 15$ nm, whose distance is much larger than that observed in our experiment.[23,24] Therefore, the influence of the water film and adsorbed contamination on dissipation may be ruled out. Secondly, the formation of chemical bonds between the atoms of the tip and sample surface will also cause huge dissipation, but such short–range interactions require that the tip-sample distance is very small enough to form chemical bonds.[21,22] However, in our experiment, friction began to increase at $d \sim 2$ nm, and there was no tunneling current when the maximum value appeared, indicating that there was no physical contact and chemical bond formation between the tip and the sample. Karrai *et al.* found that if a long probe was used, when the tip-sample distance was very small, a huge lateral interaction will make the tip bend elastically, thus generating restoring force and modulating the observed dissipation.[24] Therefore, the frequency offset will gradually stabilize as the distance decreased. The stiffness of the force sensor we used was 6 times higher than theirs, and the frequency offset detected by us maintained an increasing trend at small tip-sample separation, instead of stabilizing as observed by Karrai *et al.* Therefore, the effect of tip bending can be ruled out. Similar results can be observed in different areas of the graphite surface, excluding the influence of tip deformation on experimental results, indicating that this phenomenon is determined by the intrinsic properties of the graphite surface.

Many relaxation processes exist at the friction interface

In the equation of cantilever motion, Γ_{int} and k_{int} are expressed as[20]

$$\Gamma_{int}\dot{x} + k_{int}x = (k_{int} + i\omega\Gamma_{int})x \cong (k_{int} + i\omega_0\Gamma_{int})x \equiv G(\omega_0)x \quad (3)$$

where x is the displacement of the cantilever, and $G(\omega_0)$ is the response function. We rearranged the data in Fig. 2(b) and (c) and $\omega_0\Gamma_{int}$ as a function of k_{int} was plotted, as shown in Fig. 2(e). This is similar to what is called a Cole–Cole plot in the dielectric phenomena.[38] According to the Debye relaxation mechanism, if there is only one relaxation mechanism in the dielectric material, or a single relaxation time scale, the Cole–Cole plot will appear as a semicircle. If there are multiple relaxation mechanisms like lattice deformation and phonon excitation which will be discussed in detail in the following paragraphs, that is, the relaxation time is a distribution, the Cole–Cole plot will appear

Open Access Article. Published on 29 September 2022. Downloaded on 6/21/2026 10:24:36 AM.
This article is licensed under a Creative Commons Attribution-NonCommercial 3.0 Unported Licence.

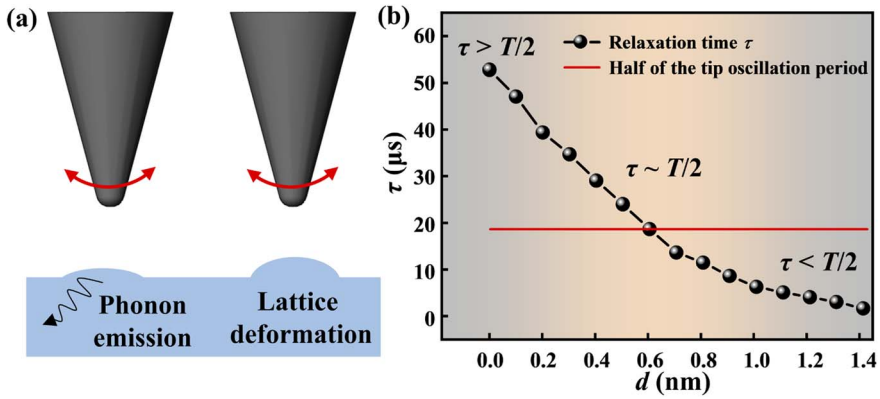

Fig. 3 (a) Model schematic diagram. The oscillation of the tip can cause the atoms on the surface of the sample to vibrate, which can excite phonons and even cause lattice deformation; (b) the mean relaxation time of atomic vibration on the graphite surface varies with the tip-sample distance. At d ~0.6 nm, the mean relaxation time is equivalent to half of the tip oscillation period, which induces significant hysteretic behavior and dissipation peaks.

as an ellipse. Based on the analogy results, we performed semicircular fitting on the experimental data, as the red lines shown in Fig. 2(e). In order to show the experimental data clearly, only the lower part of the semicircle is shown, noticing that the ranges of the x-axis and y-axis are different. The experimental data are below the semicircle and much flatter, which presents an elliptical shape. Therefore, we can attribute the observed non-contact friction phenomenon to the existence of a series of relaxation mechanisms on the graphite surface, and these relaxation processes have different relaxation time scales.

The dissipation peak is caused by the hysteretic behavior of tip oscillation and the relaxation process

To further explore the relaxation mechanism, we established the following model. The oscillation of the tip can induce some relaxation processes like atomic vibration which excites phonons and even cause lattice deformation, as shown in Fig. 3(a). Therefore, it is natural to assume that as d decreases, it becomes much easier for the atoms on the sample surface to vibrate, which can explain the dependence of non-contact friction on d. Based on this idea, we can describe the lateral interactions with a dashpot γ_f connected in series with a spring k_f. Γ_{int} and k_{int} can be expressed as[20]

$$\omega_0\Gamma_{int} = k_f\omega_0\tau/(1 + \omega_0^2\tau^2) \quad (4)$$

$$k_{int} = k_f\omega_0^2\tau^2/(1 + \omega_0^2\tau^2) \quad (5)$$

where τ is the relaxation time, which is defined as $\tau = \gamma_f/k_f$. It is assumed that the relaxation time increases as d decreases. But in fact, the vibration of the surface atoms is related to the lateral position of the atoms. Thus, atomic vibration should be represented by a distribution of relaxation time, which is why Fig. 2(e) shows an ellipse. For simplicity, we can assume that τ in the formula is an average relaxation time based on the above relaxation time distribution.

According to the expression of $\omega_0\Gamma_{int}$ and k_{int} in the model, we can solve the expression of the average relaxation time τ as

$$\tau = k_{int}/\omega_0^2\Gamma_{int} \quad (6)$$

Fig. 3(b) shows the mean relaxation time τ increase with the decrease of d with an order of tens of microseconds. Surprisingly, when the average relaxation time increases to 19 μs which is about half of the tip oscillation period, it corresponds to the position where the maximum non-contact friction occurs (d ~0.6 nm), which indicates that the energy dissipation is closely related to the mean relaxation time τ.

We propose that the non-contact friction phenomenon in the experiment can be attributed to the hysteretic behavior between the oscillation of the tip and the vibration of the surface atoms. When the tip-sample distance is large, the interaction between the tip and sample surface atoms is weak, which makes the surface atoms vibrate slightly, showing the form of phonon dissipation. Meanwhile, the average relaxation time is smaller than the oscillation period of the tip and almost no hysteretic behavior occurs. Therefore, the coupling of the two motions is weak, and the non-contact friction is also small. However, with the decrease of the distance, the vibration of the surface atoms gradually intensifies leading to a longer relaxation time. When the average relaxation time increases to half of the oscillation period of the tip, it will induce a phase shift between the oscillation of the tip and the surface atomic deformation which causes significant hysteretic behavior resulting in a huge non-contact friction peak.[39,40] As the distance decreases further, the relaxation time exceeds half of the oscillation period of the tip. The hysteretic behavior disappears and the two motions change from strong coupling to weak coupling. The smaller the distance, the weaker the coupling of the two motions and the dissipation becomes small. This hypothesis explains our experimental phenomenon very well.

Conclusions

We have studied the relationship between the energy dissipation of non-contact friction and the tip-sample distance on the graphite surface with a homebuilt tuning fork non-contact lateral force microscope in the atmosphere. It is found that

© 2022 The Author(s). Published by the Royal Society of Chemistry

Open Access Article. Published on 29 September 2022. Downloaded on 6/21/2026 10:24:36 AM.
This article is licensed under a Creative Commons Attribution-NonCommercial 3.0 Unported Licence.

energy dissipation begins to increase when the distance is less than 2 nm, which is proportional to $d^{-4.1\pm0.1}$, showing the form of phonon dissipation. However, when the distance is further reduced, the dissipation deviates from the phonon dissipation and presents a huge dissipation peak. The oscillation of the tip above the surface induces the vibration of the surface atoms, and the relaxation time of the vibration of surface atoms increases with the decrease of the tip-sample distance. At the peak position, the mean relaxation time of the surface atomic vibration has the same scale as half of the oscillation period of the tip, which induces significant hysteretic behavior and strong coupling of the two motions. However, before and after the peak position, due to the different time scales of the two motions, the hysteretic behavior and coupling is weak and the friction is small. This work provides new insights into the mechanism of non-contact friction energy dissipation.

Methods

Calibration process of the sensor

The sensor has been calibrated by analyzing the thermal noise spectrum. Sensitivity is defined as the ratio of the actual amplitude of the free cantilever of the tuning fork to the amplitude of the AC voltage signal output by the pre-amplifier. When there is no specific frequency driving signal, the free cantilever exhibits random thermal vibration, which satisfies the relation: $\frac{1}{2}kA_{\mathrm{th}}^2 = \frac{1}{2}k_{\mathrm{B}}T$, where k is the spring constant; A_{th} is the amplitude of the thermal vibration of the cantilever; k_{B} is the Boltzmann's constant. The frequency spectrum of the voltage signal corresponding to the thermal vibration can be obtained by connecting the pre-amplifier with a spectrum analyzer. By calculating the root mean square V_{th} of the signal peak, the sensitivity can be calculated as $A_{\mathrm{th}}/V_{\mathrm{th}}$.

Conflicts of interest

There are no conflicts to declare.

Acknowledgements

This work was supported by the National Natural Science Foundation of China (No. 52075284, 52105195, 51527901, and 11890672) and Postdoctoral Research Foundation of China (No. 2020M680528 and BX2021151).

References

1 O. Hod, E. Meyer, Q. Zheng and M. Urbakh, *Nature*, 2018, **563**, 485–492.
2 J. Luo, *Chin. Sci. Bull.*, 2020, **65**, 2966–2978.
3 J. B. Pendry, *J. Phys.: Condens. Matter*, 1997, **9**, 10301–10320.
4 A. I. Volokitin, B. N. J. Persson and H. Ueba, *Phys. Rev. B*, 2006, **73**, 165423.
5 M. Kisiel, E. Gnecco, U. Gysin, L. Marot, S. Rast and E. Meyer, *Nat. Mater.*, 2011, **10**, 119–122.
6 B. C. Stipe, H. J. Mamin, T. D. Stowe, T. W. Kenny and D. Rugar, *Phys. Rev. Lett.*, 2001, **87**, 096801.
7 T. D. Stowe, T. W. Kenny, D. J. Thomson and D. Rugar, *Appl. Phys. Lett.*, 1999, **75**, 2785–2787.
8 S. Kuehn, R. F. Loring and J. A. Marohn, *Phys. Rev. Lett.*, 2006, **96**, 156103.
9 M. Kisiel, F. Pellegrini, G. E. Santoro, M. Samadashvili, R. Pawlak, A. Benassi, U. Gysin, R. Buzio, A. Gerbi, E. Meyer and E. Tosatti, *Phys. Rev. Lett.*, 2015, **115**, 046101.
10 F. Federici Canova, S. Kawai, C. de Capitani, K. Kan'no, T. Glatzel, B. Such, A. S. Foster and E. Meyer, *Phys. Rev. Lett.*, 2013, **110**, 203203.
11 X. Tan, D. Guo and J. Luo, *Friction*, 2022, **10**, 748–761.
12 S. Kuehn, J. A. Marohn and R. F. Loring, *J. Phys. Chem. B*, 2006, **110**, 14525–14528.
13 S. Kuehn, R. F. Loring and J. A. Marohn, *Phys. Rev. Lett.*, 2006, **96**, 156103.
14 A. J. Weymouth, *J. Phys.: Condens. Matter*, 2017, **29**, 323001.
15 J. H. She and A. V. Balatsky, *Phys. Rev. Lett.*, 2012, **108**, 136101.
16 A. Siria, T. Barois, K. Vilella, S. Perisanu, A. Ayari, D. Guillot, S. T. Purcell and P. Poncharal, *Nano Lett.*, 2012, **12**, 3551–3556.
17 Z. Xu, Z. Jacob and T. Li, *Nanophotonics*, 2021, **10**, 537–543.
18 R. Luthi, E. Meyer, M. Bammerlin, A. Baratoff, L. Howald, C. Gerber and H. J. Guntherodt, *Surf. Rev. Lett.*, 1997, **4**, 1025–1029.
19 D. Rugar, R. Budakian, H. J. Mamin and B. W. Chui, *Nature*, 2004, **430**, 329–332.
20 K. Saitoh, K. Hayashi, Y. Shibayama and K. Shirahama, *Phys. Rev. Lett.*, 2010, **105**, 236103.
21 A. J. Weymouth, D. Meuer, P. Mutombo, T. Wutscher, M. Ondracek, P. Jelinek and F. J. Giessibl, *Phys. Rev. Lett.*, 2013, **111**, 126103.
22 F. J. Giessibl, M. Herz and J. Mannhart, *Proc. Natl. Acad. Sci. U. S. A.*, 2002, **99**, 12006–12010.
23 M. Lee, B. Kim, J. Kim and W. Jhe, *Nat. Commun.*, 2015, **6**, 7359.
24 K. Karrai and I. Tiemann, *Phys. Rev. B: Condens. Matter Mater. Phys.*, 2000, **62**, 13174–13181.
25 A. Laine, A. Vanossi, A. Nigues, E. Tosatti and A. Siria, *Nanoscale*, 2021, **13**, 1955–1960.
26 A. Nigues, A. Siria, P. Vincent, P. Poncharal and L. Bocquet, *Nat. Mater.*, 2014, **13**, 688–693.
27 B. Gotsmann, *Nat. Mater.*, 2011, **10**, 87–88.
28 M. Langer, M. Kisiel, R. Pawlak, F. Pellegrini, G. E. Santoro, R. Buzio, A. Gerbi, G. Balakrishnan, A. Baratoff, E. Tosatti and E. Meyer, *Nat. Mater.*, 2014, **13**, 173–177.
29 M. Kisiel, O. O. Brovko, D. Yildiz, R. Pawlak, U. Gysin, E. Tosatti and E. Meyer, *Nat. Commun.*, 2018, **9**, 2946.
30 D. Yildiz, M. Kisiel, U. Gysin, O. Gurlu and E. Meyer, *Nat. Mater.*, 2019, **18**, 1201–1206.
31 F. J. Giessibl, *Appl. Phys. Lett.*, 2000, **76**, 1470–1472.
32 B. Gotsmann, C. Seidel, B. Anczykowski and H. Fuchs, *Phys. Rev. B: Condens. Matter Mater. Phys.*, 1999, **60**, 11051–11061.
33 C. Loppacher, R. Bennewitz, O. Pfeiffer, M. Guggisberg, M. Bammerlin, S. Schar, V. Barwich, A. Baratoff and

© 2022 The Author(s). Published by the Royal Society of Chemistry

Open Access Article. Published on 29 September 2022. Downloaded on 6/21/2026 10:24:36 AM.
This article is licensed under a Creative Commons Attribution-NonCommercial 3.0 Unported Licence.

E. Meyer, *Phys. Rev. B: Condens. Matter Mater. Phys.*, 2000, **62**, 13674–13679.
34 G. Rubio-Bollinger, P. Joyez and N. Agrait, *Phys. Rev. Lett.*, 2004, **93**, 116803.
35 A. I. Volokitin, B. N. J. Persson and H. Ueba, *J. Exp. Theor. Phys.*, 2007, **104**, 96–110.
36 I. E. Dzyaloshinskii, E. M. Lifshitz and L. P. Pitaevskii, *Adv. Phys.*, 1961, **10**, 165–209.
37 A. I. Volokitin and B. N. Persson, *Phys. Rev. Lett.*, 2005, **94**, 086104.
38 K. S. Cole and R. H. Cole, *J. Chem. Phys.*, 1941, **9**, 341–351.
39 P. M. Hoffmann, S. Jeffery, J. B. Pethica, H. O. Ozer and A. Oral, *Phys. Rev. Lett.*, 2001, **87**, 265502.
40 L. N. Kantorovich, *Phys. Rev. B: Condens. Matter Mater. Phys.*, 2001, **64**, 245409.

© 2022 The Author(s). Published by the Royal Society of Chemistry